NANO LETTERS

2009
Vol. 9, No. 10
3430-3434

Tuning the Graphene Work Function by Electric Field Effect

Young-Jun Yu,[†,‡] Yue Zhao,[†] Sunmin Ryu,[§] Louis E. Brus,[§] Kwang S. Kim,[‡] and Philip Kim*[,†]

Department of Physics, Columbia University, New York, New York 10027, Center for Superfunctional Materials, Department of Chemistry, Pohang University of Science and Technology, Hyojadong, Namgu, Pohang 790-784, Korea, and Department of Chemistry, Columbia University, New York, New York 10027

Received May 17, 2009; Revised Manuscript Received August 20, 2009

ABSTRACT

We report variation of the work function for single and bilayer graphene devices measured by scanning Kelvin probe microscopy (SKPM). By use of the electric field effect, the work function of graphene can be adjusted as the gate voltage tunes the Fermi level across the charge neutrality point. Upon biasing the device, the surface potential map obtained by SKPM provides a reliable way to measure the contact resistance of individual electrodes contacting graphene.

High conductivity[1,2] and low optical absorption[3,4] make graphene an attractive material for use as a flexible transparent conductive electrode.[5−8] This atomically thin carbon layer provides the additional benefit that its work function can be adjusted by the electric field effect (EFE). Since the band alignment of two different materials is determined by their respective work functions, control over the graphene work function is the key to reducing the contact barriers of graphene top electrode devices.[9,10] Previous scanning probe based studies[11−13] reveal that the work function of graphene is in a similar range to that of graphite, ∼4.6 eV,[14] and depends sensitively on the number of layers.[15,16] However, the active controlling of the graphene work function has yet to be demonstrated.

In this study, we apply scanning Kelvin probe microscope (SKPM) techniques to back-gated graphene devices and demonstrate that the work function can be controlled over a wide range by EFE induced modulation of carrier concentration. SKPM is an atomic force microscope (AFM) based experimental technique that can map the surface potential variation of a sample surface relative to that of a metallic tip.[17] The change of work function is ascribed by the Fermi level shift due to the EFE induced carrier doping and is well quantified by the electronic band structure of graphene. On biased graphene devices, SKPM also allows us to accurately measure graphene/metal contact resistances by mapping the surface potential of a device. The wide range of control over the work function demonstrated here suggests graphene as an ideal material for applications where work function optimization is important.

Graphene samples were prepared by mechanical exfoliation[18] on Si wafers covered with 300 nm thick SiO_2, and then Cr/Au electrodes (5 nm/30 nm thickness) were fabricated by standard electron beam lithography. The thickness of each graphene samples was characterized by Raman spectroscopy (see Figure S1 in Supporting Information). In this work, we have studied three single layer graphene (SLG) and two bilayer graphene (BLG) transistors. Figure 1a shows a schematic diagram of the simultaneous SKPM experiments with the EFE induced carrier modulation. The SKPM measurements were performed by a commercial atomic force microscope (XE-100, Park Systems Corp.) in air and dry nitrogen environment at room temperature. During observing SKPM data, we applied an ac voltage amplitude of ∼0.3−0.5 V and a frequency of 17 kHz to a Cr/Au coated probe. The SKPM images were obtained with a two-way scan method to avoid topographic artifacts. The first scan was for topography by noncontact mode with dithering resonant frequency ∼120−170 kHz and the second scan was for SKPM image with 10−30 nm constant height mode.

The carrier density, and hence the Fermi energy, E_F, of the graphene, is controlled by the gate voltage V_g applied to the degenerately doped Si substrate. Figure 1b−e shows the optical, AFM topographic, and surface potential images of one of the SLG devices used in this experiment. In general, the local surface potential, V_{CPD}, obtained from the contact potential difference between the SKPM probe and local surface,[17] is sensitively influenced by V_g. By comparing V_{CPD}

* Corresponding author, pk2015@ columbia.edu.
† Department of Physics, Columbia University.
‡ Center for Superfunctional Materials, Department of Chemistry, Pohang University of Science and Technology.
§ Department of Chemistry, Columbia University.

10.1021/nl901572a CCC: $40.75 © 2009 American Chemical Society
Published on Web 08/31/2009

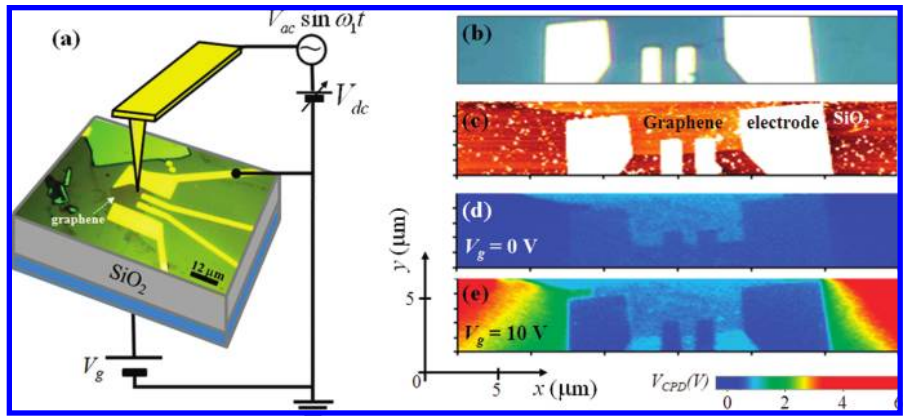

Figure 1. (a) Schematic diagram for measuring the EFE modulation of the surface potential of graphene devices using the SKPM. Gate voltage V_g is applied to the degenerately doped Si substrate and the electrodes of graphene device are grounded. (b−e) From top to down, optical image (b), AFM topography (c), and SKPM images of graphene device $V_g = 0$ V (d) and 10 V (e), respectively.

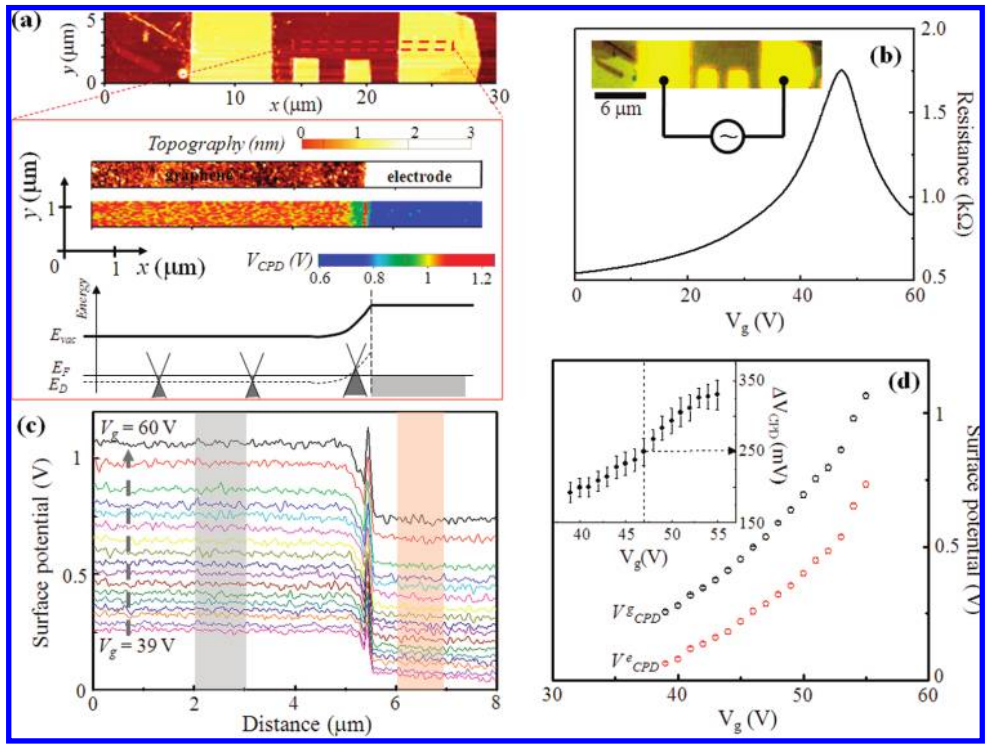

Figure 2. (a) Top panel shows an AFM topography of the device. The surface potential map of a selected area far from the graphene edges (marked by a dotted line box) is analyzed in detail in order to minimze the effect from unscreened long ranged electrostatic force from the gate. Small spatial variations in the topographic and SKPM signals are found to be correlated on the top of the graphene surface. $V_g = 55$ V in this image. A schematic energy alignment diagram for the graphene sample and the metallic elecrode is displayed where E_{vac}, E_F, and E_D are representing the vacuum energy level, Fermi energy, and the charge neutrality point of graphene, respectively. (b) Transport measurement using the two outer terminals as shown in the inset. From the peak position we have $V_D = 48$ V. (c) The surface potential profile along the x-axis (averaged over the y-axis) at different gate voltages V_g (at every 1 V from 39 to 60 V). (d) The CPD of graphene V^g_{CPD} and electrode V^e_{CPD} at different gate voltages obtained from the average surface potential in the selected gray and red shaded area in (c). The inset shows $\Delta V_{CPD} = V^g_{CPD} - V^e_{CPD}$ as a function of V_g. The vertical dashed line indicates $V_g = V_D$ where the corresponding ΔV_{CPD} is highlighted by the horizontal arrow.

maps taken at $V_g = 0$ (Figure 1d) and 10 V (Figure 1e), we notice a much larger signal contrast at higher V_g. In particular, V_{CPD} tends to increase to values comparable to V_g on the insulating SiO_2 substrate. This indicates that the unscreened electric field from the back gate is the dominant source for the contrast in V_{CPD} image in the bare SiO_2 regions. In order to minimize a direct exposure of the SKPM probe to this long-range electrostatic influence, we limit our surface potential analysis to areas within the conducting part of the device, where the subtle local surface potential variation can be readily probed.

Utilizing multiterminal device geometry, we carry out a comparison study of the surface potential (Figure 2a) and transport measurement (Figure 2b) on the same device as a function of V_g. In the particular device shown in this figure, we determine the charge neutral gate voltage $V_D = 48$ V,

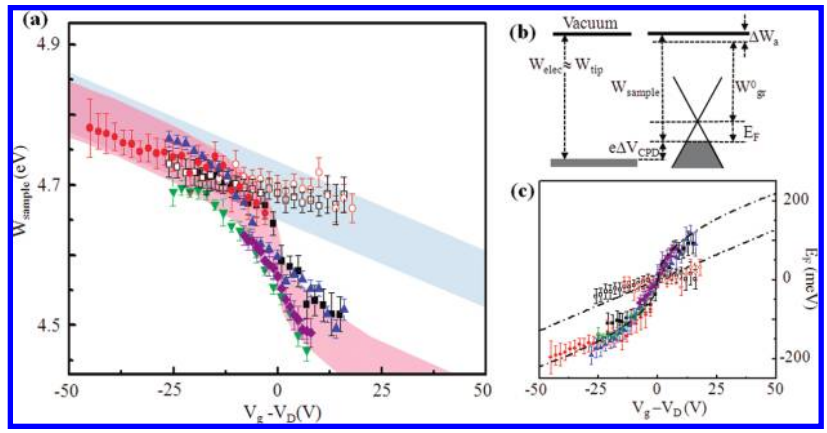

Figure 3. (a) Measured work function of SLG samples (filled symbols) and BLG samples (open symbols) as a function of $V_g - V_D$. SLG samples show larger work function changes (shaded in red) while the BLG samples exhibit fewer changes (shaded in blue), where shaded areas indicate the uncertainty for the work function offset due to the adsorbate induced surface dipole layers (see Supporting Information). The filled green, red, and purple symbols are SLG data taken in air. Other data were taken in a dry nitrogen environment. (b) Schematic diagram for the energy level alignment in the SKPM tip and graphene samples. The left panel shows the work function of tip relative to the vacuum level. The right panel shows the relation between W_{sample}, W^0_{gr}, E_F, and ΔW_a, defined in the text relative to the vacuum level. (c) The Fermi energy variation of SLG and BLG as a function of $V_g - V_D$. Symbols are same as in (a). E_F is deduced from W_{sample}, by subtracting off $W^0_{gr} + \Delta W_a$, whose values obtained at the charge neutrality point $V_g = V_D$. The dashed curve and line are the E_F^{SLG} and E_F^{BLG} from the band structure calculations.

from the gate voltage corresponding to a sharp resistance peak. In the surface potential map where V_g is fixed, we observe a stepwise increase of V_{CPD} at the junctions between graphene and electrodes regions, but no significant spatial variation within each region. Similar features are observed at different values of V_g (Figure 2c), where the overall line profiles of V_{CPD} in the two regions shift upward with a common background as V_g increases. This background signal is due to the unscreened long-range electrostatic interaction between the conducting cantilever probe and the back gate and, thus, is insensitive to a small spatial position change of the SKPM tip. Since V_g should not influence the local surface potential in metallic electrode, the background signal on the metal electrode surface can serve to separate the spatially constant background from the relative change in the local surface potential. In particular, the EFE induced local surface potential change in graphene, ΔV_{CPD}, can be obtained by $\Delta V_{CPD} = V^g_{CPD} - V^e_{CPD}$, where V^e_{CPD} and V^g_{CPD} are the average V_{CPD} in the electrode and the graphene, respectively (Figure 2d, inset). Interestingly, a sudden change ΔV_{CPD} is observed at the charge neutrality point ($V_g = V_D$), as indicated by the vertical dashed line. Similar features are always present at the neutrality point in other SLG samples studied in this experiment. We also perform similar measurement of ΔV_{CPD} on BLG samples. Similar to the SLG, ΔV_{CPD} of BLG can be modulated by applied gate voltage (see Figure S2 in Supporting Information). Unlike the SLG samples, however, there is no such sudden change of ΔV_{CPD} at the BLG charge neutrality point, implying the difference of the electronic structures of the samples as we will discuss later.

The relative surface contact potential difference, ΔV_{CPD} obtained above can be related to the difference in work function between two different surfaces: $e\Delta V_{CPD} = W_{elec} - W_{sample}$, where W_{elec} and W_{sample} are work functions of the electrode and graphene sample surfaces, respectively. Since W_{elec} is insensitive to V_g due to the large density of states near the Fermi level in the gold electrodes, the observed variation of $\Delta V_{CPD}(V_g)$ reflects the EFE modulation of W_{sample}. We note that the work function of our gold-coated tip is close to W_{elec} since both the SKPM probe and the electrodes are made of gold and that they are exposed in the same experimental condition. A separately performed calibration measurement yields $W_{tip} = 4.82 \pm 0.08$ eV (see Figure S3 in Supporting Information). Using this value, we estimate $W_{sample} \approx W_{tip} - e\Delta V_{CPD}$. Figure 3a shows the resulting W_{sample} as a function of $\Delta V_g = V_g - V_D$. Here we list results obtained from several SLG and BLG devices in different experimental conditions. For each data set, the transport characteristics are measured independently to obtain V_D. We found that V_D ranges from 30 to 50 V for most devices. The positive sign of V_D indicates that the samples are hole doped from the environment, suggesting a dipole layer formation on the top of graphene surface. Despite this uncontrolled environment doping, we demonstrate that the work function of sample can be tuned by EFE within the range 4.5−4.8 eV for SLG and 4.65−4.75 eV for BLG in ambient and dry nitrogen conditions. With further optimization using chemcial functionalization, a wide range of work functions can potentially be achieved for applications which require adjustment of the work function.

The behavior of EFE tuned W_{sample} can be explained by the change of E_F in graphene devices. From the schematic diagram in Figure 3b, we note $W_{sample} = \Delta W_a + W^0_{gr} - E_F$, where ΔW_a is the offset of work function due to the adsorbate dipole layer formation and $W_{gr}{}^0$ is the intrinsic work function of undoped graphene. In order to estimate $W_{gr}{}^0$ from the measured W_{sample}, an independent estimation of ΔW_a is necessary. In the experiments performed in air and dry nitrogen atmosphere, we estimated $|\Delta W_a| < 50$ meV for both SLG and BLG (see Figure S4 in Supporting Information). This upper bound of $|\Delta W_a|$ allows us to estimate the work functions of undoped SLG and BLG from the measured

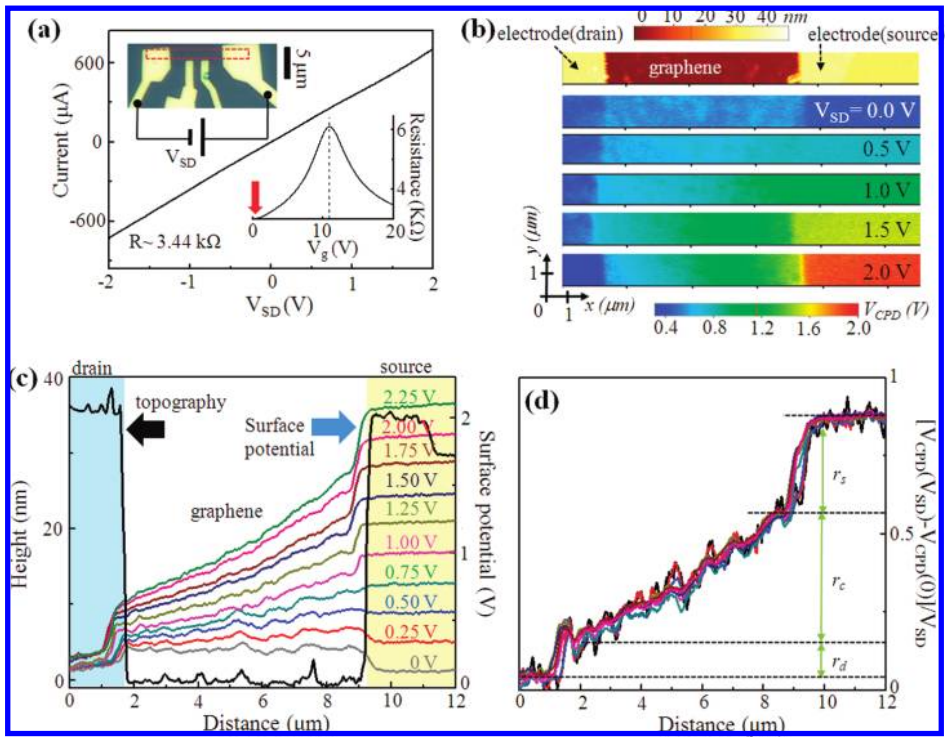

Figure 4. (a) Current (I) and bias voltage (V_{SD}) characteristic of a SLG device. The slope of the curves indicates the two terminal resistance of device (3.44 kΩ). Upper inset shows the optical microscope image of the device. Lower inset shows the resistance as a function of V_g. The vertical arrow indicates the gate voltages and dotted line, V_D. (b) Topographic AFM image (top) and surface potential images of the area marked by the red rectangular box in (a). The drain electrode is grounded while the source electrode is biased by V_{SD} as indicated in each panel. The gate voltage is fixed to $V_g = 0$. (c) Surface potential profiles along the x-axis shown in (b) at different V_{SD}. (d) Normalized and referenced surface potential profiles shown in (c). The surface potential referenced to the grounded drain electrode (V_{CPD} ($V_{SD} = 0$)) and normalized by V_{SD}. All the curves shown in (c) are collapsed in a single curve, where distinct kinks appear due to the contact resistances between electrodes and graphene. The proportion of the source and drain contact resistances and the channel resistance are marked by r_s, r_d, and r_c, respectively.

$W_{sample}(\Delta V_g = 0)$. With this analysis, we obtained $W_{gr}^0 = 4.57 \pm 0.05$ eV for SLG and 4.69 ± 0.05 eV for BLG, which are in reasonable agreement with recent theoretical estimations.[19−21] Note that the work function of SLG is found to be smaller than that of BLG, indicating the chemical stability of BLG over SLG.[22]

The controlled modulation of W_{sample} allows us to estimate the EFE induced E_F variation. Noting that $E_F(\Delta V_g{=}0) = 0$ in our convention, we have $E_F(\Delta V_g) = W_{sample}(\Delta V_g{=}0) - W_{sample}(\Delta V_g)$. Figure 3c shows E_F (ΔV_g) calculated from the data sets displayed in Figure 3a. Remarkably, five data sets from SLG and two data sets from BLG all collapse into two separate families of the curves representing E_F (ΔV_g) for SLG and BLG, respectively. The Fermi energy variation of SLG and BLG can be described by the change of carrier density induced by the EFE, i.e., $E_F^{SLG} = \mathrm{sign}(\Delta V_g)\hbar v_F(\alpha\pi|\Delta V_g|)^{1/2}$ for SLG and $E_F^{BLG} = \hbar^2\pi\alpha\Delta V_g/2m^*$ for BLG, where $\alpha = 7.1 \times 10^{10}$ cm^{-2} V^{-1} is the gate capacitance in electron charge, $v_F = 1 \times 10^6$ m/s is the Fermi velocity of SLG, and $m^* = 0.033m_e$ is the effective mass of carrier in BLG relative to the bare electron mass m_e obtained from the literature.[23−25] Employing these values, we plot E_F^{SLG} (dashed curve) and E_F^{BLG} (dashed line) in Figure 3c, where excellent agreements are found without any fitting parameters, indicating the observed work function variation is ascribed solely to the EFE modulation of E_F.

Finally, we discuss the simultaneous SKPM surface potential mapping on graphene devices with a finite bias voltage V_{SD} applied between two electrodes. Figure 4a shows the current (I) versus V_{SD} characteristics at a fixed gate voltage. The slope of $I-V_{SD}$ yields a resistance of 3.44 kΩ which includes the contributions of contact resistances between each electrode and the graphene channel. The simultaneous SKPM surface potential mapping provides a way to estimate these contributions independently. Figure 4b displays topographic and surface potential mapping of the same device with increasing V_{SD} from 0 to 2 V. The surface potential of the grounded source electrode remains close to 0 V, while the surface potential of the biased drain electrode shifts upward as V_{SD} increases. From the horizontal profile of these images (Figure 4c), we clearly observe linearly increasing V_{CPD} in the channel and kinks in V_{CPD} at the junctions. We attribute these sudden potential drops to the contact resistance between the electrodes and graphene. By taking the grounded drain electrode as the reference point (V_{CPD} ($V_{SD} = 0$)) and normalizing the V_{CPD} by V_{SD}, all the surface potential profiles at different V_{SD} collapse into one universal curve $[V_{CPD}(V_{SD}) - V_{CPD}(V_{SD} = 0)]/V_{SD}$ (Figure 4d). The vertical ratios between the kinks and the slope correspond to the source and drain contact resistances (r_s and r_d) and graphene channel resistance (r_c). Considering that the total two terminal resistance of this device is 3.44

kΩ, we obtain r_d:r_c:r_s = 0.5:1.7:1.24 kΩ for this particular device.

In conclusion, by employing a gate modulated SKPM measurement, we have demonstrated that the work function of graphene can be substantially adjusted by EFE. This widely tunable work function makes graphene an attractive material for low contact barrier electrodes. The simultaneous SKPM surface potential imaging allows us to evaluate the contacts of graphene devices.

Acknowledgment. We thank Mark S. Hybertsen for helpful discussion. This work was supported by DOE (No. DEFG02-05ER46215, DE-FG02-98ER-14861), ONR (N000140610138), NSF NSEC (No. CHE-0117752), NYSTAR, FENA MARCO center, DARPA (FA8650-08-C-7838) through CERA program, KICOS(GRL), KOSEF (EPB Center: R11-2008-052-01000), and BK21(KRF).

Supporting Information Available: Optical images and Raman spectroscopy of single-layer graphene (SLG) and bilayer graphene (BLG) for confirming thickness, the surface potential modulation of a BLG device by the change of gate voltage, the calibration of the work function of SKPM probes, and work function offset of SLG and BLG. This material is available free of charge via the Internet at http://pubs.acs.org.

References

(1) Bolotin, K.; Sikes, K. J.; Jiang, Z.; Klima, M.; Fudenberg, G.; Hone, J.; Kim, P.; Stomer, H. L. *Solid State Commun.* **2008**, *146*, 351–355.
(2) Du, X.; Skachko, I.; Barker, A.; Andrei, E. Y. *Nat. Nanotechnol.* **2008**, *3*, 491–495.
(3) Nair, R. R.; Blake, P.; Grigorenko, A. N.; Novoselov, K. S.; Booth, T. J.; Stauber, T.; Peres, N. M.; Geim, A. K. *Science* **2008**, *320*, 1308.
(4) Mak, K. F.; Sfeir, M. Y.; Wu, Y.; Lui, C. H.; Misewich, J. A.; Heinz, T. F. *Phys. Rev. Lett.* **2008**, *101*, 196405.
(5) Li, X.; Zhang, G.; Bai, X.; Sun, X.; Wang, X.; Wang, E.; Dai, H. *Nat. Nanotechnol.* **2008**, *3*, 538–542.
(6) Eda, G.; Fanchini, G.; Chhowalla, M. *Nat. Nanotechnol.* **2008**, *3*, 270–274.
(7) Reina, A.; Jia, X.; Ho, J.; Nezich, D.; Son, H.; Bulovic, V.; Dresselhaus, M. S.; Kong, J. *Nano lett.* **2009**, *9*, 30–35.
(8) Kim, K. S.; Zhao, Y.; Jang, H.; Lee, S. Y.; Kim, J. M.; Kim, K. S.; Ahn, J.-H.; Kim, P.; Choi, J.-Y.; Hong, B. H. *Nature* **2009**, *457*, 706–710.
(9) Ishii, H.; Sugiyama, K.; Ito, E.; Seki, K. *Adv. Mater.* **1999**, *11*, 605–625.
(10) Jiang, J.; Krauss, T. D.; Brus, L. E. *J. Phys. Chem. B* **2000**, *104*, 11936–11941.
(11) Filleter, T.; Emtsev, K. V.; Seyller, Th.; Bennewitz, R. *Appl. Phys. Lett.* **2008**, *93*, 133117.
(12) Datta, S. S.; Strachan, D. R.; Mele, E. J.; Johnson, A. T. C. *Nano Lett.* **2009**, *9*, 7–11.
(13) Shi, Y.; Dong, X.; Chen, P.; Wang, J.; Li, L.-J. *Phys. Rev. B* **2009**, *79*, 115402.
(14) Takahashi, T.; Tokailin, H.; Sagawa, T. *Phys. Rev. B* **1985**, *32*, 8317–8324.
(15) Giovannetti, G.; Khomyakov, P. A.; Brocks, G.; Karpan, V. M.; Van den Brink, J.; Kelly, P. J. *Phys. Rev. Lett.* **2008**, *101*, 026803.
(16) Hibino, H.; Kageshima, H.; Kotsugi, M.; Maeda, F.; Guo, F.-Z.; Watanabe, Y. *Phys. Rev. B* **2009**, *79*, 125437.
(17) Rosenwaks, Y.; Shiker, R.; Glatzel, Th.; Sadewasser, S. *Phys. Rev. B* **2004**, *70*, 085320.
(18) Novoselov, K. S.; Jiang, D.; Schedin, F.; Booth, T. J.; Khotkevich, V. V.; Morozov, S. V.; Geim, A. K. *Proc. Natl. Acad. Sci. U.S.A.* **2005**, *102*, 10451–10453.
(19) Shan, B.; Cho, K. *Phys. Rev. Lett.* **2005**, *94*, 236602.
(20) Ooi, N.; Rairkar, A.; Adams, J. B. *Carbon* **2006**, *44*, 231–242.
(21) Sque, S. J.; Jones, R.; Briddon, P. R. *Phys. Status Solidi* **2007**, *204*, 3078–3084.
(22) Liu, L.; Ryu, S.; Tomasik, M. R.; Stolyarova, E.; Jung, N.; Hybertsen, M. S.; Steigerwald, M. L.; Brus, L. E.; Flynn, G. W. *Nano Lett.* **2008**, *8*, 1965–1970.
(23) Li, Z. Q.; Henriksen, E. A.; Jiang, Z.; Hao, Z.; Martin, M. C.; Kim, P.; Stomer, H. L.; Basov, D. N. *Nat. Phys.* **2008**, *4*, 532–535.
(24) Henriksen, E. A.; Jiang, Z.; Tung, L.-C.; Schwartz, M. E.; Takita, M.; Wang, Y.-J.; Kim, P.; Stormer, H. L. *Phys. Rev. Lett.* **2008**, *100*, 087403.
(25) Yan, J.; Henriksen, E. A.; Kim, P.; Pinczuk, A. *Phys. Rev. Lett.* **2008**, *101*, 136804.

NL901572A